HHS Public Access

Author manuscript

J Am Soc Mass Spectrom. Author manuscript; available in PMC 2017 February 01.

Published in final edited form as:

J Am Soc Mass Spectrom. 2016 February ; 27(2): 285–292. doi:10.1007/s13361-015-1283-y.

Dynamic Reactive Ionization with Cluster Secondary Ion Mass Spectrometry

Hua Tian[1], **Andreas Wucher**[2], and **Nicholas Winograd**[1]

Hua Tian: hut3@psu.edu

[1]Chemistry Department, Pennsylvania State University, University Park, PA 16802, USA

[2]Fakultät für Physik, Universität Duisburg–Essen, 47048, Duisburg, Germany

Abstract

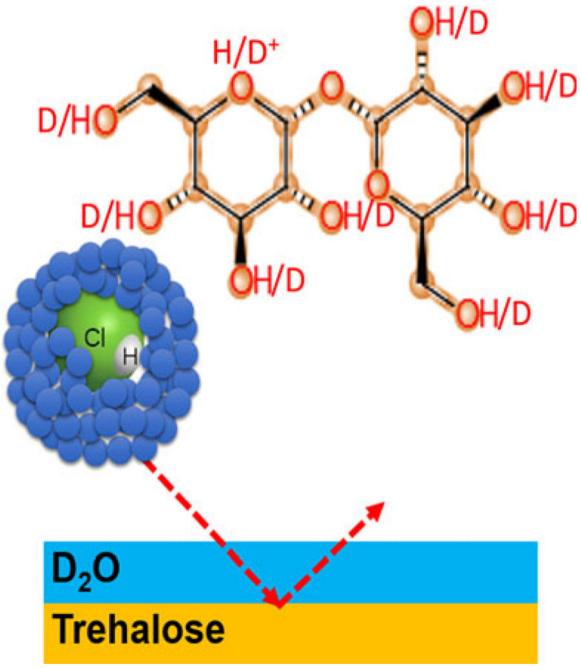

Gas cluster ion beams (GCIB) have been tuned to enhance secondary ion yields by doping small gas molecules such as CH_4, CO_2, and O_2 into an Ar cluster projectile, Ar_n^+ (n = 1000–10,000) to form a mixed cluster. The ‘tailored beam’ has the potential to expand the application of secondary ion mass spectrometry for two- and three-dimensional molecular specific imaging. Here, we examine the possibility of further enhancing the ionization by doping HCl into the Ar cluster. Water deposited on the target surface facilitates the dissociation of HCl. This concerted effect, occurring only at the impact site of the cluster, arises since the HCl is chemically induced to ionize to H^+ and Cl^-, allowing improved protonation of neutral molecular species. This hypothesis is confirmed by depth profiling through a trehalose thin film exposed to D_2O vapor, resulting in ~20-

Correspondence to: Hua Tian, hut3@psu.edu.

Electronic supplementary material The online version of this article (doi:10.1007/s13361-015-1283-y) contains supplementary material, which is available to authorized users.

fold increase in protonated molecules. The results show that it is possible to dynamically maintain optimum ionization conditions during depth profiling by proper adjustment of the water vapor pressure. Protonation and H–D exchange in the trehalose molecule M was monitored upon deposition of D_2O on the target surface, leading to the observation of $[M_n^* + H]^+$ or $[M_n^* + D]^+$ ions, where n = 1–8 hydrogen atoms in the trehalose molecule M have been replaced by deuterium. In general, we discuss the role of surface chemistry and dynamic reactive ionization of organic molecules in increasing the secondary ion yield.

Keywords

Cluster secondary ion mass spectrometry; Dynamic reactive ionization; GCIB; Ar cluster

Introduction

The emergence of gas cluster ion beams (GCIB) for secondary ion mass spectrometry (SIMS) experiments has opened new opportunities for fragment-free mass spectrometry, imaging, and molecular depth profiling [1]. Several groups, employing an argon cluster primary ion source typically consisting of 1000–10,000 Ar atoms, have attempted to find optimized conditions for minimizing sample damage and optimizing the ion yield from organic substrates [2–7]. Computer simulations, empirical models, and experimental results have suggested that an impact energy of ~5 eV per atom is a value that yields minimal sample damage, yet provides excellent depth profiles, either directly or in combination with other beams such as Bi_3^+ [7–10]. There is a fundamental conundrum associated with this situation, however, since parameters pointing toward reduced sample damage also result in low ionization probabilities. Hence, the major application of GCIB has been as a sputter erosion source rather than as a desorption probe for secondary ion mass spectrometry (SIMS) experiments [11]. The full potential of these large clusters still remains to be tapped.

Although improving ionization probability is a longstanding goal, not only for SIMS experiments but for all mass spectrometry methods, it is especially critical for GCIBs since they are inherently poor at generating secondary ions [12]. A range of strategies has been employed to overcome this problem for a wide range of primary ion projectiles. For example, matrices employed in MALDI experiments have been particularly useful in boosting the intensity of higher mass secondary ions, presumably through proton donation to form the protonated molecule, $[M + H]^+$. Salt addition can, under some conditions, improve ionization through adduct formation [13]. Similarly, Cs flooding or Cs^+ bombardment enhances ionization through $[M + Cs]^+$ formation [14, 15]. Several groups have employed the strategy of using H_2O as a source of protons, particularly since it is the natural matrix of biological materials. Simple flooding of the sample with H_2O has been shown to be effective at increasing ionization of many organic compounds [16–18]. Acidification of H_2O by gas-phase HCl also enhances protonated molecule formation [19, 20]. Of special interest here is the use of a H_2O cluster ion beam consisting of several thousand H_2O molecules [12, 21]. For this probe, ionization efficiencies are observed to increase by an order of magnitude over comparably-sized Ar GCIB, and studies with D_2O suggest that the incorporated proton is indeed being supplied, at least in part, by the primary ion.

With this background, it has been our strategy to dope the Ar GCIBs with chemically active species, which may assist in the ionization process [22]. There are several potential advantages of this approach. Reactive molecules, entrained in the cluster, will be delivered precisely to the point of desorption at the correct time. During impact, they may be kinetically activated via dissociation or fragmentation to form radicals, which then can interact with sputtered molecules. Moreover, projectile induced surface chemistry can be tuned by varying the composition of the GCIB. And finally, since the concentration of the reactive species in the GCIB is low (<10%), damage to vacuum lines and pumps is kept to a minimum and the cluster formation process is largely unperturbed.

Here, we investigate HCL as a dopant acid in the GCIB. By itself, the cluster may not have enough energy upon cluster impact to break the H–Cl bond efficiently or, if it is broken, the dissociation products would be H and Cl atoms. Preliminary experiments using such a projectile have shown that for a target consisting of a thin film of trehalose, the intensity of the $[M + H]^+$ ion was virtually unchanged (see Supplementary Figure S2 in the Supporting Information). A possible solution to this problem might be to entrain HCl into an H_2O cluster ion beam, where the dissociation to H_3O^+ and Cl^- is an exothermic process. Issues associated with the reactive gas vapor necessary to form the cluster in the ion source itself, unfortunately, render this approach to be impractical.

In this work, we combine neutral HCl doped into an Ar GCIB with D_2O adsorbed onto the bombarded surface. Deuterated water in the form of deposited ice is employed so that the source of protons can be more clearly identified. With this scheme, acidic reactions are restricted to the point of impact, precisely where they are needed to facilitate the ionization of a sputtered molecule. The results show that the presence of HCl in the cluster increases the secondary ion signal from D_2O cluster ions in the ice layer by more than a factor of 1000, confirming our basic hypothesis. This ionization enhancement mechanism is referred to as dynamic reactive ionization (DRI).

Experimental

Sample Preparation

D-(+)-trehalose dehydrate (BioReagent, ≥99%, Sigma, Saint Louis (MO), USA) was dissolved into HPLC water at a concentration of 0.5 M. A 100 μL trehalose solution was spin-coated onto a pre-cleaned (rinsed consecutively in chloroform, water, and methanol) Cu substrate (5 × 5 mm^2) using a spin coater (Laurell Technologies, North Wales (PA), USA, model: WS-650-23NPP) at 5000 rpm. To form a smooth film on the Cu surface, a 10 μL trehalose aliquot was repeatedly dropped onto the substrate 10 times at 20 s intervals while the substrate spun, followed by drying for 3 min. The samples were then mounted onto a Cu sample block (4 cm × 3 cm × 1.5 cm) and inserted into the instrument under the protection of N_2 gas.

SIMS Experiment

To evaluate the ionization of Ar GCIBs, the trehalose film was analyzed under different conditions by SIMS using a J105 3D Chemical Imager by Ionoptika [23, 24]. The

experiments utilized primarily two different ion beams consisting of either 20 keV Ar_{2000}^+ or 20 keV HCl doped Ar_{2000}^+ clusters. The beams were generated using a GCIB source from Ionoptika. The source was operated at a beam current of ~90 pA and was focused to a spot diameter of ~3 0 μm. The cluster size distribution was centered around 2000 with a width of ±500 constituents. The procedure used to dope small amounts of reactive gas into the Ar GCIB has been described in detail elsewhere [25]. Provisions were made to ensure that the pure and doped GCIB had similar ion current and focal dimensions. All experiments reported here were acquired using a doping level of 5% HCl added to the Argon gas supply driving the GCIB.

Depth profiles of the trehalose film were firstly performed at room temperature with both the pure and HCl doped Ar GCIB in positive and negative SIMS mode. Depth profiling was performed via the sequential acquisition of 32 × 32 pixel images with the ion beam operated in pulsed mode at a duty cycle of 50% and rastered over an area of 400 × 400 μm^2. The ion fluence accumulated during each of these cycles (subsequently referred to as “layers”) was 1.8×10^{12} ions/cm^2 for both ion beams. According to the universal equation describing the sputtering yield of organic material under GCIB bombardment [7], the sample volume removed per impact of a cluster composed of 2000 constituent units (Ar atoms or HCl molecules) with 20 keV kinetic energy should be ~53 nm^3. This value corresponds to removal of ~1 nm during each layer of acquisition. The film itself was typically 60–80 nm in thickness. The sample was then cooled to 110 K inside the analysis chamber, and depth profiles were repeated on fresh areas of the surface. Subsequently, D_2O was injected into the vacuum chamber via a controllable leak valve connected to a small glass vial containing about 1 cm^3 of D_2O (≥99.95%, Acros). For some of the experiments, ice overlayers were deposited on top of the trehalose film by exposing the cold sample to a D_2O partial pressure of 3×10^{-7} mbar for 20 min. Depth profiles of the resulting ice-trehalose film were performed again on fresh areas of the sample. At least two parallel analyses were completed for each depth profiling condition. All experiments were also repeated on separate days. Finally, the precooled surface of trehalose was exposed to D_2O during depth profiling, and the optimum surface condition was determined by adjusting the D_2O partial pressure. In these experiments, five layers were first acquired without the presence of D_2O, then the D_2O pressure was ramped up gradually to a maximum of 1.26×10^{-6} mbar in the analysis chamber.

Ice Deposition

The deposition of an ice film on a surface at temperature T requires the partial pressure of water in the vacuum system to be larger than the equilibrium vapor pressure at this temperature. The vapor pressure of water in the temperature range relevant in these experiments is shown in Supplementary Figure S4. Owing to technical restrictions, the maximum pressure in our system is 2×10^{-6} mbar, which means that the surface temperature must be below 150 K in order to allow the growth of an ice overlayer. The growth rate attainable under these conditions is ~0.3–0.5 nm/s.

Data Processing

Data were processed using the Ionoptika Image Analyzer (ver. 1.0.6.12) software. The intensity of protonated and deprotonated molecules, major fragment ions and D_2O/HCl-induced peaks were plotted as a function of the analysis cycles or “layers” as defined above. The ion intensity was determined by digitization of the output of a channel plate detector system via a Fast Flight II recording system [23].

Results and Discussion

The goal of this work is to investigate the role of surface chemistry induced by the combination of cluster projectile constituents with a surface water-ice overlayer. In particular, we address the question of whether such a protocol may be used to enhance the useful signal of protonated molecules during a sputter depth profile through a molecular film. The route towards this goal consists of a number of sequential steps, which will be discussed separately.

Ice Overlayer Depth Profiles

Typical mass spectra obtained from a D_2O ice overlayer deposited on top of the trehalose surface are shown in Supplementary Figure S5. Spectra acquired from an ice overlayer directly deposited onto the copper substrate yield similar results. Data taken from the freshly prepared surface (layer 1) and after sputter removal of a few nm (layer 10, but still well within the ice film) show that pure and HCl doped Ar GCIBs generate vastly different spectra. In particular, the total ion signal from the original ice surface (layer 1) produced by the HCl doped clusters is an order of magnitude larger than that produced by pure Ar clusters. This effect becomes even more pronounced after sputter erosion to layer 10, which generates an increase in ion signal for the HCl doped clusters, while the signal from the pure Ar GCIB becomes barely detectable. The positive ion spectra are dominated by water cluster ions of the type $[D_2O]_n^+$, $[D_2O]_nH^+$, or $[D_2O]_nD^+$, respectively. The peaks are split into groups and separated by one mass unit with different intensity distributions for both projectiles. An example is depicted in the inset of Supplementary Figure S5a, which shows the ions $[D_2O]_5^+$, $[D_2O]_5H^+$, and $[D_2O]_5D^+$ at *m/z* 100, 101, and 102, respectively, and ions at *m/z* 96, 97, 98, and 99, which correspond to an exchange of 4, 3, 2, or 1 deuterium atoms with the corresponding number of hydrogen atoms. The intensity of these peaks increases with increasing ion fluence while employing the HCl doped GCIB, but completely disappears when using the Ar GCIB. This finding shows that the hydrogen atoms replacing the deuterium atoms originate from the HCl contained in the projectile. Hence, there must be a chemical reaction of the projectile dopant with surface water molecules, presumably associated with exothermic dissociation of neutral HCl that is mixed into the Ar cluster. Once the ions are formed, they are available for attachment to ejected water clusters, resulting in enhanced ionization.

For the negative spectra, the analysis is more complicated, since both projectiles generate entirely different spectra. The spectrum generated by the pure Ar GCIB in layer 1 is dominated by peaks that are spaced by 13–16 mass units and appear not to be correlated with water clusters but rather with a hydrocarbon surface contamination. Virtually no signal

remains by the time layer 10 is reached. The spectrum generated by the HCl doped GCIB, on the other hand, exhibits peak groups that are spaced by 20 mass units and therefore are clearly related to ejected water clusters of the type $[D_2O]_nO^-$, $[D_2O]_nOH^-$, or $[D_2O]_nOD^-$ with varying numbers of D–H exchanges. An example is shown in the inset of Supplementary Figure S5b, which depicts this progression for n = 5. The prominent signals at *m/z* 208 and 209 correspond to a cluster of 10 water molecules associated with an O^- or OH^- anion for ionization, where eight of the 20 D atoms in the cluster have been exchanged with H. This observation again indicates that there is an intimate reaction between HCl and the surface water.

These findings are further supported by examining the fluence dependence of the water cluster signals. Depth profiles obtained for a few major water cluster ion peaks are shown in Figure 1. The profiles acquired with the HCl doped GCIB show a rapid transition into a quasi-steady state with approximately constant ion intensities, until the ice film is removed after ~35 layers. In contrast, the ice film is practically unobservable when employing the pure GCIB. To demonstrate that the rapid signal drop observed in this case is not induced by a corresponding drop of the sputter yield and that the ice film is still being eroded, the $[M-OH]^+$ signal of trehalose at *m/z* 325 is included in the plot. These findings indicate that the observed signal decay must reflect a change in the ionization probability of the sputtered water clusters, which is obviously absent when the HCl doped projectile is employed.

Trehalose Depth Profiles

We begin the discussion with depth profiles of the trehalose film at room temperature as shown in Supplementary Figure S3. The profiles measured with the Ar GCIB closely resemble those obtained earlier [25]. The positive ion signals in the mass region of the molecular ion are dominated by $[M + Na]^+$ and $[M-OH]^-$ ions, with the $[M + H]^+$ intensity ~10-fold below the $[M-OH]^-$ value. In this notation and throughout the remainder of this paper, M refers to the intact trehalose molecule at *m/z* 342. The negative ion spectrum is clearly dominated by the $[M-H]^-$ ion peak. After an initial drop by ~2-fold, all of these signals reach a quasi-steady state as described by the erosion dynamics model [22].

The profiles obtained with the HCl doped Ar GCIB exhibit a slightly different behavior. In the positive ion spectrum, all signals appear to be higher than those obtained with the pure GCIB. The ion signals in the mass region of the molecular ion exhibit the same ordering, but after the initial signal drop the $[M + Na]^+$ intensity is found to increase while the $[M-OH]^+$ and $[M + H]^+$ intensity decreases in the quasi-steady state region. Hence, the spectrum becomes more and more dominated by the sodium adduct ion peak. This observation indicates that the signal variation is not due to accumulated damage but rather reflects changes in the ionization probability of the sputtered molecules. Apparently, the Na concentration in the film must increase with decreasing distance to the Cu substrate, promoting sodiation versus protonation as the dominant ionization mechanism. We speculate that the origin of this effect might be an adventitious NaCl salt residue at the Cu substrate prior to trehalose deposition, leading to the consistent observation of a maximum of the $[M + Na]^+$ intensity at that interface. The negative ion spectrum at this interface is dominated by

an $[M + Cl]^-$ adduct ion peak, and the $[M-H]^-$ ion formation becomes suppressed by ~5-fold.

If the sample stage is cooled to liquid nitrogen temperature, one obtains the profiles depicted in Figure 2. In general, the data look similar to those measured at room temperature (see Supplementary Figure S3), but there are a few notable differences. First, the positive ion spectrum measured with the HCl doped Ar GCIB is no longer dominated by the $[M + Na]^+$ signal, since its intensity has been suppressed by nearly a factor of six in the steady state. Moreover, the initial signal drop observed with the pure Ar GCIB appears to be much more pronounced than for the room temperature profiles. Concomitantly, the $[M + Cl]^-$ signal now exhibits an initial signal increase instead of the decrease observed at room temperature. In view of observations discussed below, these changes are most likely attributable to a small amount of adventitious H_2O that has been adsorbed at the surface during the cooling process. Finally, all negative ion signals are reduced relative to those found for the room temperature profile, and the $[M-H]^-$ signal appears to be even more strongly suppressed when using the HCl doped Ar GCIB than with the pure Ar GCIB as shown in Supplementary Figure S3. The origin of these differences remains unclear at the present time.

D_2O on Trehalose

Typical depth profiles measured for the D_2O|trehalose system are shown in Figure 3. The D_2O overlayer, the interface to the underlying trehalose film, and the transition to the Cu substrate are clearly discernible. With the pure Ar GCIB, all water cluster ions rapidly decay in intensity during the removal of the ice overlayer as noted above. When approaching the interface between the ice and the trehalose film, the ion signals at *m/z* 325 ($[M-OH]^+$), 341 ($[M-H]^-$), 343 $(M + H)^+$), 365 ($[M + Na]^+$), and 377 ($[M + Cl]^-$) rapidly increase and reach a steady state with intensity levels comparable to those found for the dry trehalose film. If the HCl doped Ar GCIB is used, the interface between trehalose and the Cu substrate is marked by a rapid increase of the $[Cu_2H]^+$ and $[CuCl_2]^-$ signals, both of which are negligible when using the pure Ar GCIB.

Probably the most interesting feature of the profiles measured with the HCl doped Ar GCIB is the occurrence of pronounced maxima for a number of positive and negative ions at the interface between the ice overlayer and the trehalose film. In the positive ion spectrum, groups of peaks spaced by one mass unit are observed, beginning at *m/z* 325, 344, and 365. In the negative ion spectrum there is a similar group starting at *m/z* 377. An example of the mass spectrum measured at the interface maximum is depicted in the Supporting Information, which shows in Supplementary Figure S6 that the trehalose related ion peaks are easily distinguished from the neighboring water cluster ion peaks. As with the ice profile, we interpret these peak groups as reflecting the exchange of one or more H atoms in the trehalose molecule by D atoms. To simplify the discussion, the nomenclature M_n* with n = 1–8 will be used to describe the exchange, where n hydrogen atoms have been replaced by deuterium. Since $[M_n* + D]^+$ ions cannot be distinguished from $[M_{n+1}* + H]^+$ ions, we will in the following use the nomenclature $[M_n* + H/D]^+$ to describe the protonated molecules. Hence, there are a large number of peaks within the families of $[M_n*-OH]^+$, $[M_n* + H/D]^+$,

$[M_n^* + Na]^+$, and $[M_n^* + Cl]^-$. By correcting the measured signal intensities for the ^{13}C satellite contribution as well as the $^{35}Cl/^{37}Cl$ isotopic abundance, the probability distribution for the number of D–H exchanges can be determined. It is evident that the resulting probability distribution must depend upon the D_2O surface concentration and can, therefore, be expected to change while eroding across the ice/trehalose interface. Qualitatively, one would expect more D atoms to be found at higher D_2O concentration levels (i.e., within earlier regions of the interface where the residual D_2O concentration is still larger). A more detailed view of the corresponding profiles in this region is shown in Figure 4. It is seen that the maxima are indeed shifted toward larger depth with decreasing number of D atoms, with the maxima at the largest depth being found for the $[M_1^* + H]^+$ or $[M + D]^+$ and the $[M_1^* + Cl]^-$ signal, respectively. Note that no interface maxima are observed with the pure Ar GCIB, strongly supporting the assumption that the surface chemistry induced by the HCl dopant in the projectile is responsible for the enhanced ionization.

In order to estimate the magnitude of the ionization enhancement, it is of interest to sum the intensities of all peaks within one group. For the example depicted in Figure 4, summing the maximum intensities measured for the $[M_n^* + H/D]^+$ peak group yields about 30 times the steady state value of the $[M + H]^+$ signal measured with the pure Ar GCIB. In fact, the summed signal of this group is now larger than that for the $[M_n^* + Na]^+$ group, which means that the protonation efficiency achieved with the HCl doped Ar GCIB has been increased by more than an order of magnitude and is now comparable or even larger than the cationization efficiency.

D_2O Flooding

Although the experiments with the D_2O overlayer clearly show that surface chemistry can be used to enhance ionization, this configuration is not particularly suited to imaging or depth profiling of biological samples. It is feasible, however, to dynamically deposit a water layer on the sample during spectral acquisition to allow both of these modalities to be implemented. The idea is to establish and maintain an optimum concentration of water/ice at the surface throughout the entire depth profile, which corresponds to the conditions of the interface maxima in Figure 4. In doing so, the sample is again cooled to ~110 K, and water vapor is leaked into the analysis chamber at a controllable partial pressure. In principle, the water/ice surface concentration established under these conditions should be the result of a dynamic equilibrium between sputter removal and adsorption/ condensation of D_2O, which can be controlled by variation of the water partial pressure as well as the current density and duty cycle of the projectile ion beam.

The result of such an experiment is shown in Figure 5. While depth profiling the trehalose film with the HCl doped Ar GCIB, the D_2O partial pressure in the chamber was varied at the positions marked by the vertical lines. The mass spectra corresponding to the $[M_n^*-OH]^+$, $[M_n^* + H/D]^+$, and $[M_n^* + Na]^+$ ion signals measured at the points marked by the vertical arrows are shown in Figure 6. The molecular ions again form peak groups, reflecting the D–H exchange that was observed at the D_2O/trehalose interface. Moreover, the statistical distribution of the peak intensities within each group changes as a function of the D_2O

partial pressure. At higher pressure, the equilibrium D_2O surface coverage is larger and, hence, the probability of replacing more H atoms with D atoms becomes larger.

Consequently, the distribution shifts to higher masses as the D_2O pressure is increased between the removal of layer 11 and layer 45. A detailed description of a simple model to calculate the resulting peak intensity distribution can be found in the Supporting Information (section S5). The last spectrum in the bottom panel of Figure 6 refers to the end point of the profile, where the D_2O gas inlet has been closed long enough for the system to return to the steady state conditions without D_2O coverage. Under these conditions, the peak groups collapse into the single $[M-OH]^+$, $[M + H]^+$, and $[M + Na]^+$ peaks again as expected. As discussed in the Supporting Information (section S5), the additional peaks observed in the vicinity of the $[M + H]^+$ peak correspond to a trehalose–copper chloride adduct fragment.

To judge the signal enhancement obtained under different surface conditions, the peak areas were summed over the respective peak groups as shown in Figure 5. It is seen that under the prevailing bombarding conditions, ionization via $[M_n* + H/D]^+$ (i.e., the “protonated” molecule) formation overtakes that via $[M_n* + Na]^+$ formation at a D_2O partial pressure of 3×10^{-7} mbar. If the pressure is increased further, the protonated molecule signal increases faster than the $[M_n*-OH]^+$ signal, until at a D_2O partial pressure of 10^{-6} mbar both signals become comparable. Under these optimized conditions, the ionization efficiency via protonation has increased by an order of magnitude as compared to the dry surface bombarded with the HCl doped Ar cluster, and even more in comparison to the dry surface analyzed with the pure Ar GCIB. If the experiment is repeated with a preexisting D_2O ice overlayer, the ionization efficiency under optimized conditions is larger than at the ice/trehalose interface maxima without D_2O flooding (see Supplementary Figure S7). Note that the ionization efficiency via cationization with Na^+ remains practically unchanged, so that protonation is now strongly favored. The moderate increase of the $[M_n*-OH]^+$ signal is presumably caused by the reaction of HCl with OH groups of the trehalose molecule, which may act to enhance the probability for abstraction of water leading to the formation of a protonated $[M_n*-H_2O]H^+$ ion.

The results presented can be compared with data obtained using a pure water GCIB. Using $(H_2O)_n^+$ (n = 1000–10,000) projectiles and isoenergetic Ar_n^+ (n = 1000–6000) projectiles on similar trehalose films as investigated here, Sheraz et al. have comprehensively studied the influence of H_2O upon changing the ionization competition between $[M + Na]^+$, $[M + H]^+$, and $[M-OH]^+$ [12]. By varying the mean cluster size at a constant impact energy of 20 keV, it was found that when the impact energy per cluster constituent (H_2O molecules or Ar atoms) becomes less than ε = 10 eV, $[M + H]^+$ formation is strongly favored under water cluster ion bombardment and even becomes comparable to $[M-OH]^+$ formation at ε~3 eV, where the maximum signal levels of $[M + H]^+$ and $[M-OH]^+$ are observed. Below this value, protonation overtakes $[M-OH]^+$ formation, but both signals are found to strongly decrease again. These results suggest that optimized ionization conditions obtained under water cluster ion bombardment are characterized by comparable efficiency for $[M + H]^+$ and $[M-OH]^+$ formation. With the HCl doped Ar GCIB used here, we find a similar signal ratio under optimized water coverage conditions, albeit at ε = 10 eV, indicating that similar ionization conditions can be reached both ways. In comparing the absolute ion yields

obtained in both experiments, one has to keep in mind that the signals presented in Figure 3 of ref. [12] were obtained at the beginning of a depth profile (i.e., with an ion fluence of 5×10^{11} ions/cm^2, whereas the data presented here (Figure 5) refer to the steady state region of the depth profile, where the protonated molecule signal has already been reduced because of the buildup of some surface damage (see Figure 2). Also, it is possible that the presence of Cl^- ions somewhat limits the benefit arising from the enhanced protonation efficiency, since these ions might react with a protonated molecule and, hence, lead to ion suppression effects as demonstrated previously by the Vickerman group [13]. However, Cl^- might react with other fragment ions from trehalose, leaving a high chance of formation of protonated molecules, which we have observed in the experiment.

For the pure Ar GCIB, on the other hand, the sodiated adduct ion formation is the preferred ionization mechanism regardless of the value of ε. For 20 keV Ar_{2000}^+, an $[M + Na]^+/[M + H]^+$ signal ratio of around 100 was found in ref. [12] in good agreement with our observation here. If NaCl is deliberately added to the solution from which the trehalose film is deposited, the $[M + Na]^+$ signal increases by about a factor five and saturates at that level, while the $[M + H]^+$ and $[M-OH]^+$ signals further decrease with increasing salt content (see Supplementary Figure S1). The same projectile doped with HCl, however, generates a significantly increased protonated molecule signal at the same value of ε. In combination with a surface water layer, the dopant obviously improves the protonation efficiency in a similar way as reducing the impact energy per H_2O molecule under pure water cluster bombardment.

Conclusions

Here we show that HCl, carried by an energetic Ar GCIB, chemically reacts with surface water, leading to the formation of ionic radicals, which enhance the ionization probability via protonation. Based upon a model experiment involving the deposition of an ice overlayer on a trehalose film and subsequent depth profiling through the overlayer/trehalose interface, we conclude that the combined action of the projectile dopant and the water overlayer leads to an increase in the trehalose ionization efficiency. In addition, we show that optimum ionization conditions can be dynamically established and maintained by exposing the surface at low temperature to a controllable water partial pressure during the depth profile. In principle, the equilibrium water/ice coverage can be controlled by the H_2O partial pressure and the erosion rate, thus providing a wide range of possible combinations.

In general, the results demonstrate that surface chemistry induced by the combination of a reactively doped cluster ion beam and a suitable gas-phase reactant may open a promising route to improve the ionization efficiency in molecular SIMS. Clearly, many other types of doped clusters should be investigated using this protocol. Although we have focused upon trehalose as a model system, this ionization mechanism should be applicable to any organic molecule ionized via protonation. A further advantage of this approach is that the reaction and, hence, the acidification leading to ionization enhancement occurs only at the impact site of the projectile, where it can have the most influence on the ionization of sputtered molecules. The use of a HCl doped water cluster or a pure HCl GCIB, for example, would place severe constraints on the vacuum system and the operation of the cluster ion source.

Finally, the DRI modality should be well-suited for three-dimensional imaging of biomaterials, especially since water is often a desirable matrix for these systems.

Supplementary Material

Refer to Web version on PubMed Central for supplementary material.

Acknowledgments

The authors thank Peter Williams for reminding them about the role of water in the dissociation of HCl. This study was financially supported by the National Institutes of Health (grant no. 9R01 GM113746-20A1) and Novartis Pharmaceuticals. Infrastructure support from the Department of Energy (grant no. DE-FG02-06ER15803) is also acknowledged.

References

1. Ninomiya S, Ichiki K, Yamada H, Nakata Y, Seki T, Aoki T, Matsuo J. Molecular depth profiling of multilayer structures of organic semiconductor materials by secondary ion mass spectrometry with large argon cluster ion beams. Rapid Commun. Mass Spectrom. 2009; 23:3264–3268. [PubMed: 19757450]
2. Bich C, Havelund R, Moellers R, Touboul D, Kollmer F, Niehuis E, Gilmore IS, Brunelle A. Argon cluster ion source evaluation on lipid standards and rat brain tissue samples. Anal. Chem. 2013; 85:7745–7752. [PubMed: 23875833]
3. Gnaser H, Ichiki K, Matsuo J. Sputtered ion emission under size-selected Ar-n(+) cluster ion bombardment. Surf. Interface Anal. 2013; 45:138–142.
4. Rabbani S, Barber AM, Fletcher JS, Lockyer NP, Vickerman JC. TOF-SIMS with argon gas cluster ion beams: A comparison with C_{60}^{+}. Anal. Chem. 2011; 83:3793–3800. [PubMed: 21462969]
5. Shard AG, Havelund R, Seah MP, Spencer SJ, Gilmore IS, Winograd N, Mao D, Miyayama T, Niehuis E, Rading D, Moellers R. Argon cluster ion beams for organic depth profiling: Results from a VAMAS interlaboratory study. Anal. Chem. 2012; 84:7865–7873. [PubMed: 22897795]
6. Tian H, Wucher A, Winograd N. Molecular imagingof biological tissue using gas cluster ions. Surf. Interface Anal. 2014; 46:115–117. [PubMed: 26207076]
7. Seah MP, Havelund R, Gilmore IS. Universal equation for argon cluster size-dependence of secondary ion spectra in SIMS of organic materials. J. Phys. Chem. C. 2014; 118:12862–12872.
8. Paruch RJ, Garrison BJ, Mlynek M, Postawa Z. On Universality in sputtering yields due to cluster bombardment. J. Phys. Chem. Lett. 2014; 5:3227–3230. [PubMed: 26276337]
9. Angerer TB, Blenkinsopp P, Fletcher JS. High energy gas cluster ions for organic and biological analysis by time-of-flight secondary ion mass spectrometry. Int. J. Mass Spectrom. 2015; 377:591–598.
10. Gnaser H, Ichiki K, Matsuo J. Sputtered ion emission under size-selected Ar_n^{+} cluster ion bombardment. Surf. Interface Anal. 2013; 45:138–142.
11. Rading D, Moellers R, Cramer HG, Niehuis E. Dual beam depth profiling of polymer materials: comparison of C_{60} and Ar cluster ion beams for sputtering. Surf. Interface Anal. 2013; 45:171–174.
12. Sheraz née Rabbani S, Razo IB, Kohn T, Lockyer NP, Vickerman JC. Enhancing ion yields in time-of-flight secondary ion mass spectrom-etry: a comparative study of argon and water cluster primary beams. Anal. Chem. 2015; 87:2367–2374. [PubMed: 25588151]
13. Piwowar AM, Lockyer NP, Vickerman JC. Salt effects on ion formation in desorption mass spectrometry: an investigation into the role of alkali chlorides on peak suppression in time-of-flight-secondary ion mass spec-trometry. Anal. Chem. 2009; 81:1040–1048. [PubMed: 19125566]
14. Niehuis E, Grehl T, Kollmer F, Moellers R, Rading D, Kersting R, Hagenhoff B. MCs+ depth profiling using cluster primary ions. Surf. Interface Anal. 2011; 43:204–206.

15. Wittmaack K. Unravelling the secrets of Cs controlled secondary ion formation: Evidence of the dominance of site specific surface chemistry, alloying and ionic bonding. Surf. Sci. Rep. 2013; 68:108–230.
16. Mouhib T, Delcorte A, Poleunis C, Bertrand P. Organic ion yield enhancement in secondary ion mass spectrometry using water vapour injection. Surf. Interface Anal. 2013; 45:46–49.
17. Conlan XA, Lockyer NP, Vickerman JC. Is proton cationization promoted by polyatomic primary ion bombardment during time-of-flight secondary ion mass spectrometry analysis of frozen aqueous solutions? Rapid Commun. Mass Spectrom. 2006; 20:1327–1334. [PubMed: 16555365]
18. Roddy TP, Cannon DM, Ostrowski SG, Ewing AG, Winograd N. Proton transfer in time-of-flight secondary ion mass spectrometry studies of frozen-hydrated dipalmitoylphosphatidylcholine. Anal. Chem. 2003; 75:4087–4094. [PubMed: 14632121]
19. Donsig HA, Herridge D, Vickerman JC. Static SIMS studies of reactions on mimics of polar stratospheric clouds II: low-temperature, low-pressure interactions of Cl-2 and Cl2O with solid ice films. J. Phys. Chem. A. 1998; 102:2302–2308.
20. Donsig HA, Vickerman JC. Dynamic and static secondary ion mass spectrometry studies of the solvation of HCl by ice. J. Chem. Soc. Faraday Trans. 1997; 93:2755–2761.
21. Sheraz née Rabbani S, Barber A, Fletcher JS, Lockyer NP, Vickerman JC. Enhancing secondary ion yields in time-of-flight secondary ion mass spectrometry using water cluster primary beams. Anal. Chem. 2013; 85:5654–5658. [PubMed: 23718847]
22. Wucher A, Winograd N. Molecular sputter depth profiling using carbon cluster beams. Anal. Bioanal. Chem. 2010; 396:105–114. [PubMed: 19649771]
23. Fletcher JS, Rabbani S, Henderson A, Blenkinsopp P, Thompson SP, Lockyer NP, Vickerman JC. A new dynamic in mass spectral imaging of single biological cells. Anal. Chem. 2008; 80:9058–9064. [PubMed: 19551933]
24. Hill R, Blenkinsopp P, Thompson S, Vickerman J, Fletcher JS. A new time-of-flight SIMS instrument for 3D imaging and analysis. Surf. Interface Anal. 2011; 43:506–509.
25. Wucher A, Tian H, Winograd N. A mixed cluster ion beam to enhance the ionization efficiency in molecular secondary ion mass spectrometry. Rapid Commun. Mass Spectrom. 2014; 28:396–400. [PubMed: 24395507]

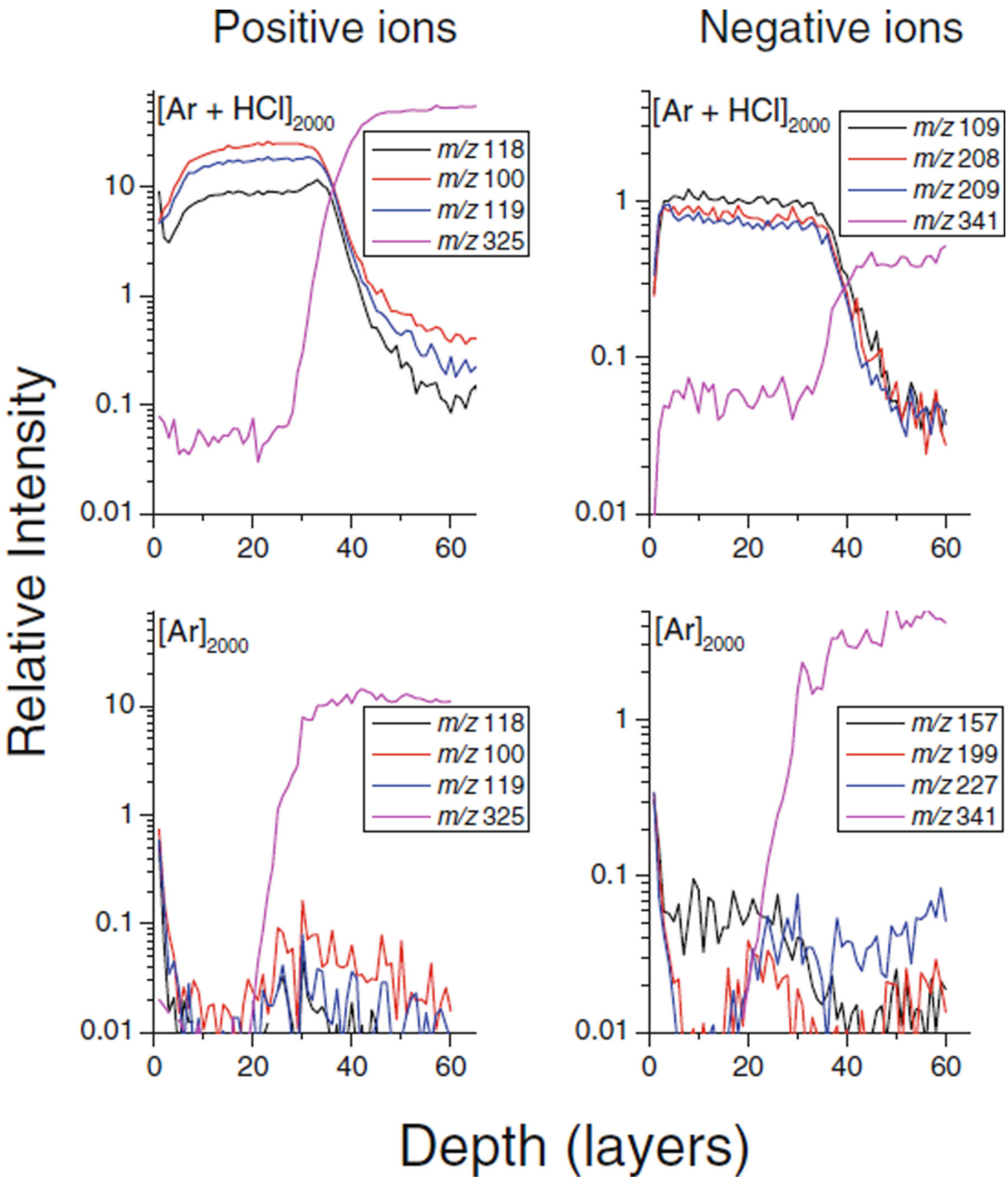

Figure 1.

Molecular depth profiles of positive and negative water cluster ion peaks at *m/z* 100, 118, 119 (positive) and 109, 208, 209 (negative) measured for a D_2O ice overlayer deposited onto a trehalose film. The signals at *m/z* 325 (positive) and 341 (negative) correspond to $[M-OH]^+$ and $[M-H]^-$ ions of trehalose

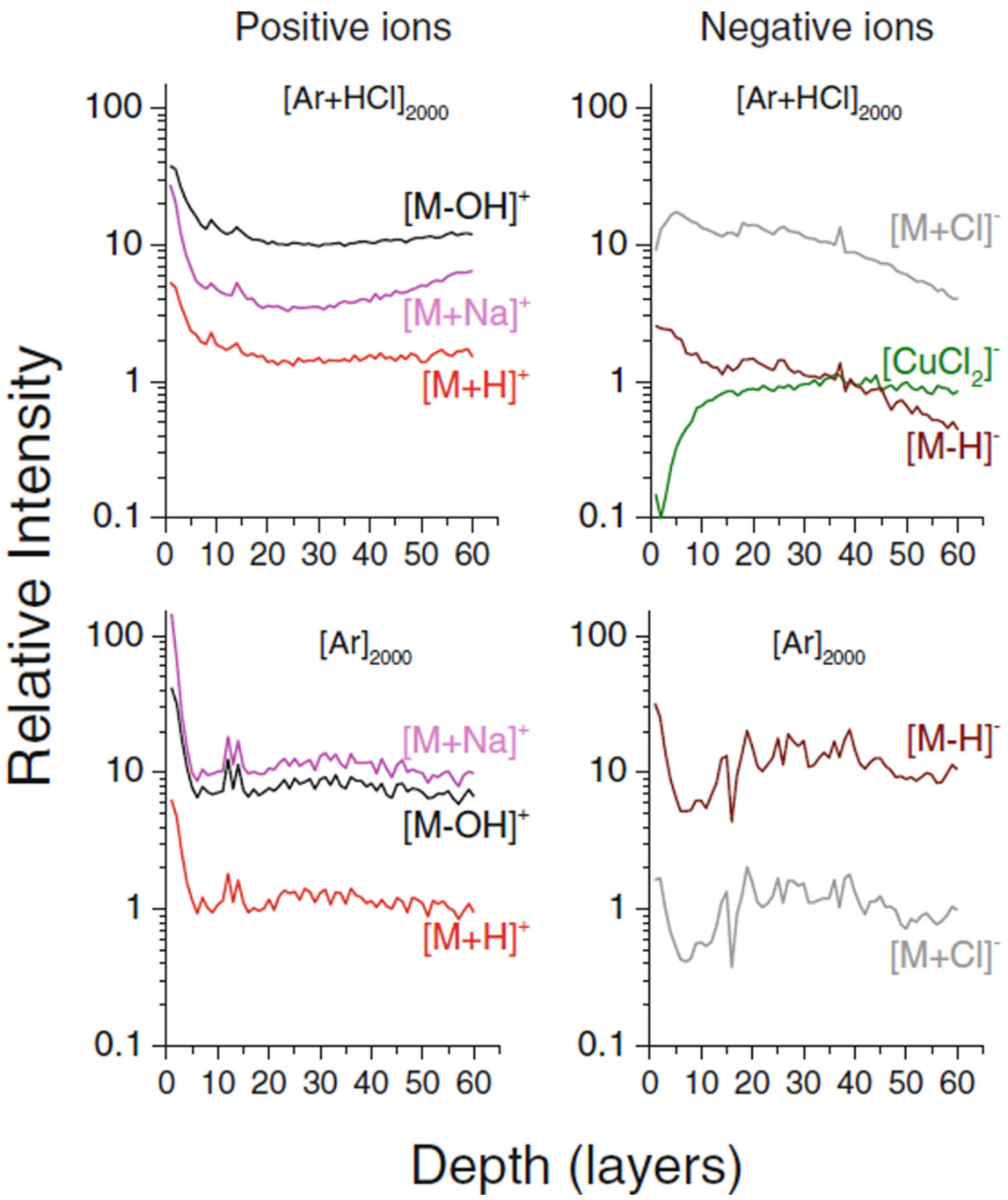

Figure 2.

Molecular depth profiles of secondary ions emitted from a trehalose film on Cu under bombardment with a HCl doped Ar_{2000} and a pure Ar_{2000} GCIB, respectively. The data were taken at 110 K without any addition of water

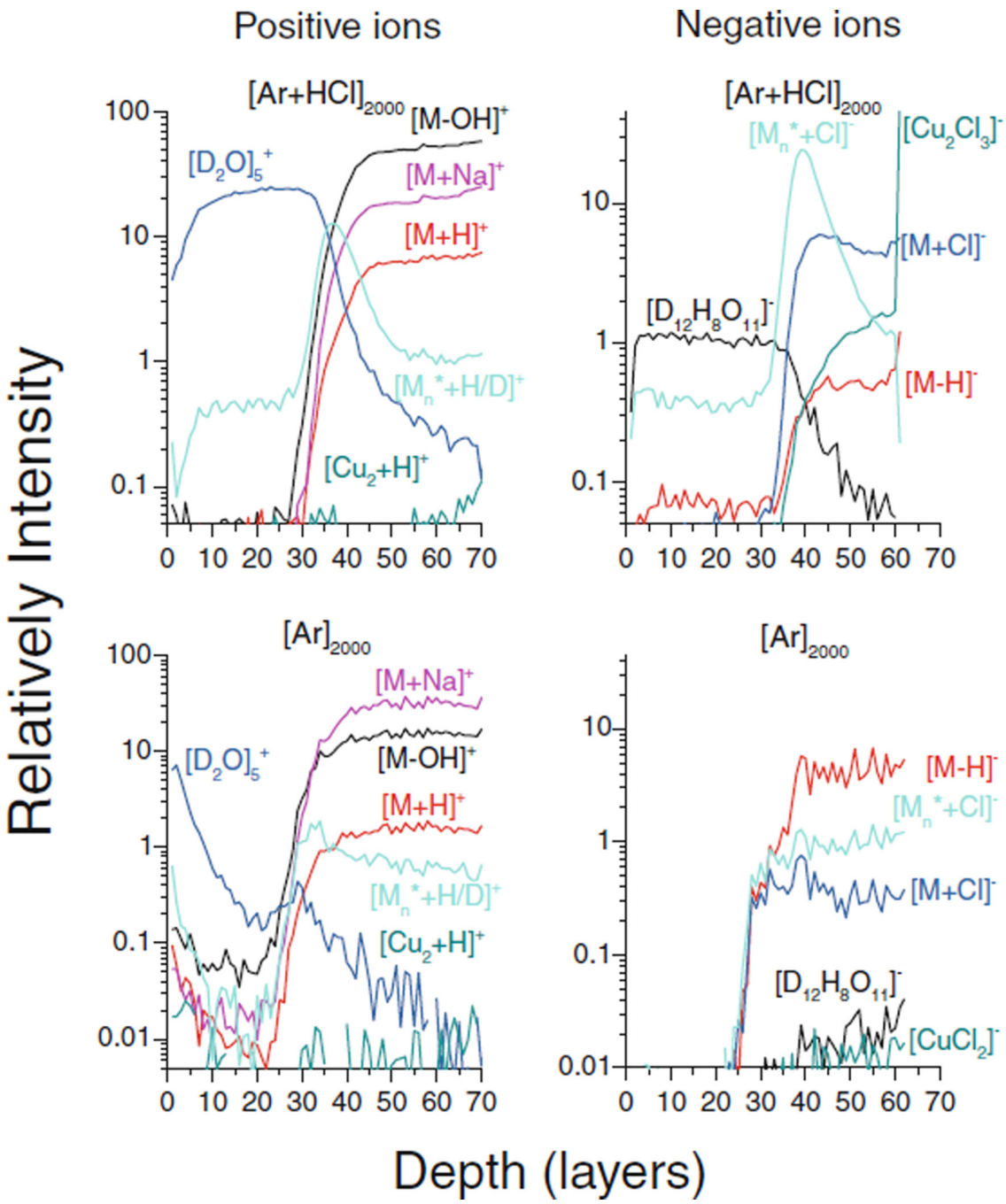

Figure 3.

Depth profiles of selected secondary ion signals measured on a trehalose film on Cu capped with a D_2O overlayer. The notation M_n* describes the exchange of H and D in the trehalose molecule M, where n H atoms have been replaced by D atoms, and the curves labeled $[M_n^* + H/D]^+$ and $[M_n^* + Cl]^-$ denote the sum of all such signals (*m/z* 344 + … + 349 and *m/z* 380 + … + 387, respectively). Note the maxima occurring for these signals near the 40 layer point associated with the water/trehalose interface are only present with the HCl doped Ar_{2000} GCIB

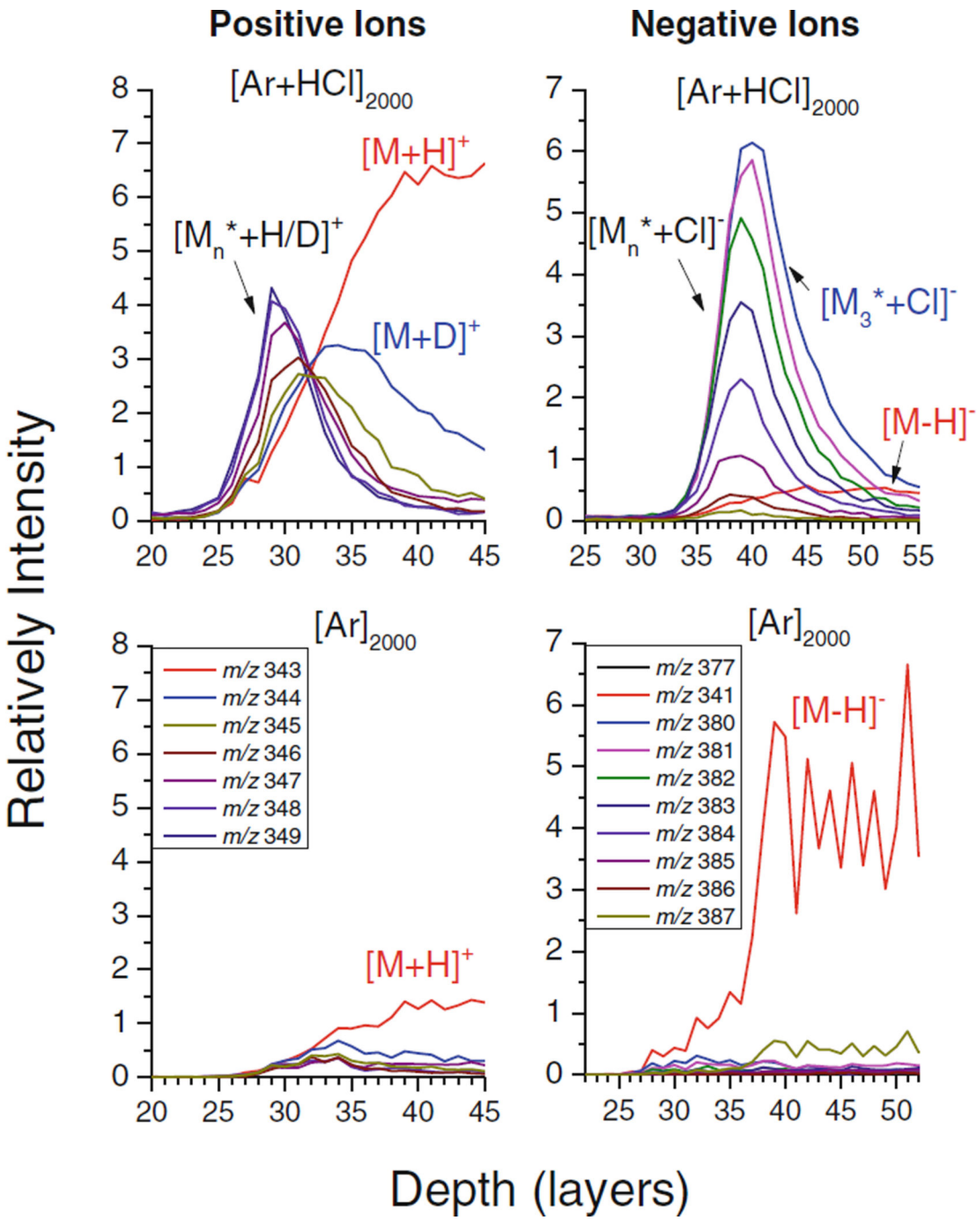

Figure 4.

Enlarged view of the profiles produced using the HCl doped Ar_{2000} GCIB as shown in Figure 3. The notation M_n* with n = 1–6 (positive ions) and n = 3–10 (negative ions) describes the exchange of H and D in the trehalose molecule M, where n hydrogen atoms have been replaced by deuterium

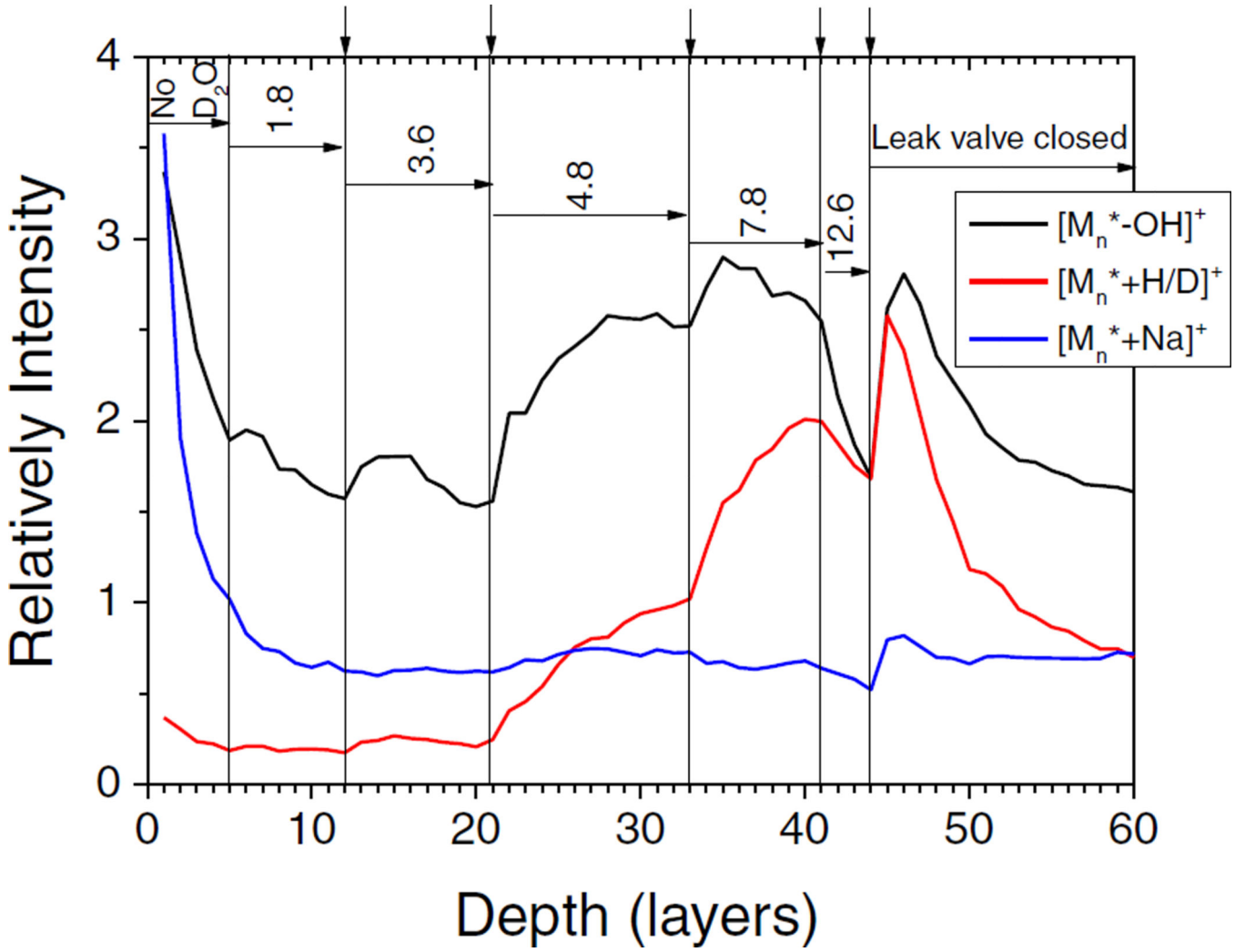

Figure 5.

Summed signal of peak groups displayed in Figure 6 corresponding to $[M_n^*-OH]^+$, $[M_n^* + H/D]^+$, and $[M_n^* + Na]^+$ (n = 1–8, for definition of M_n^* see Figure 4) versus eroded depth while profiling through a trehalose film on copper with an HCl doped Ar_{2000} GCIB at 110 K under simultaneous flooding with D_2O at different partial pressures. The vertical lines mark the times at which the flooding gas partial pressure was changed, the numbers denote the D_2O partial pressure in units of 10^{-7} mbar

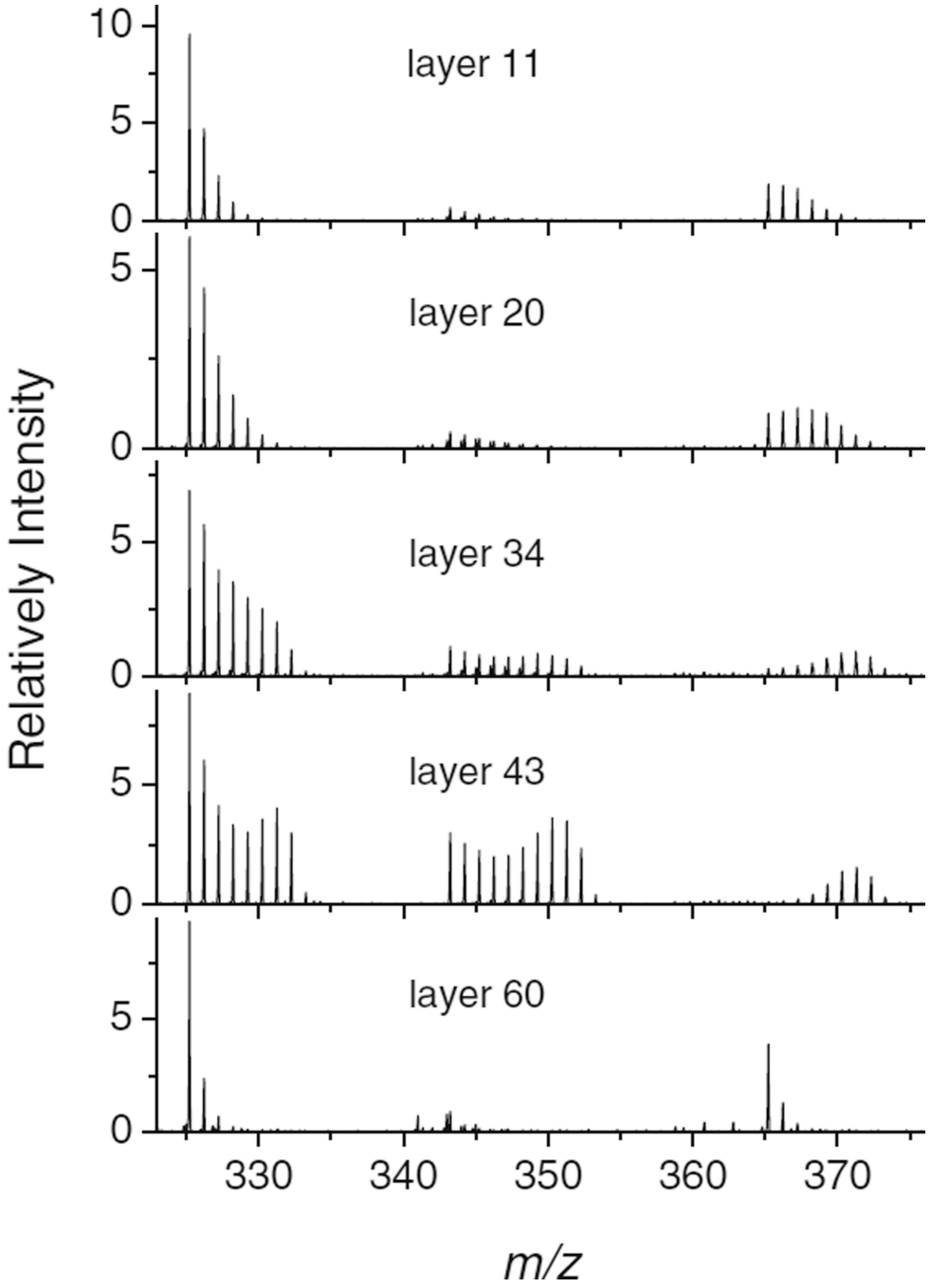

Figure 6.

Mass spectra measured at the designated points of the dynamical depth profile displayed in Figure 5. The data were taken with the HCl doped Ar_{2000} GCIB at 110 K under simultaneous flooding with D_2O at different partial pressures. The three displayed peak groups correspond to the $[M_n^*-OH]^+$, $[M_n^* + H/D]^+$, and $[M_n^* + Na]^+$ (for the definition of M_n^* see Figure 4) secondary ion signals